Desalination and Water Treatment
www.deswater.com

doi: 10.5004/dwt.2021.27112

223 (2021) 380–392
May

Removal of Yellow HE4G dye from aqueous solutions using synthesized Mn-doped PbS (PbS:Mn) nanoparticles

Shirin Bouroumand, Farzaneh Marahel*, Fereydoon Khazali

Department of Chemistry, Omidiyeh Branch, Islamic Azad University, Omidiyeh, Iran, email: Farzane.marahel.fm@gmail.com (F. Marahel), Boromand 011@gmail.com (S. Bouroumand), Khazali@iauo.ac.ir/fereydoon840@gmail.com (F. Khazali)

Received 30 November 2020; Accepted 4 February 2021

ABSTRACT

The applicability of the synthesized pure and $PbS_{(1-x)}Mn_x$ (x = 0%, 5%, 10%, and 15%) nanoparticles as a novel adsorbent for eliminating Yellow HE4G dye from aqueous media was investigated. Various techniques including Brunauer–Emmett–Teller, Fourier transform infrared, X-ray diffraction, and scanning electron microscopy were used to characterize this novel adsorbent. Via employment of a batch adsorption technique, the impact values of 10 mg/L, 0.1 g, 2.0, and 15 min were considered as the ideal values for HE4G dye, adsorbent mass, pH value, and contact time, respectively. To investigate the equilibrium behavior of adsorbent Langmuir and Freundlich models were used. Adsorption mechanism for these adsorbents was considered to be physical which was confirmed by the E (kJ/mol) obtained from the Dubinin–Radushkevich isotherm for PbS, PbS/Mn-5%, PbS/Mn-10%, and PbS/Mn-15% were roughly –700.0, –770.1, –817.12, and –903.0 (kJ/mol), respectively. Kinetics experiments were performed to investigate the adsorption kinetics. The pseudo-second-order kinetics coincided quite with the kinetic results. The maximum adsorption capacity of the HE4G dye for PbS, PbS/Mn-5%, PbS/Mn-10%, and PbS/Mn-15% were roughly 78.74, 103.9, 133.33, and 144.49 mg/g, respectively. The thermodynamic parameters including enthalpy, entropy, and Gibbs energy were calculated for the adsorption of these HE4G dye using Mn-doped PbS nanoparticles suitable, spontaneous and exothermic.

Keywords: Adsorption capacity; Yellow HE4G dye; Isotherms; Thermodynamic; Kinetic

1. Introduction

The textile dyeing industries apply synthetic dyes for the coloration of their products along with the large quantity of water and discharge the wastewater to the water bodies and environment. Dyes are chemically stable and non-degradable. Some dyes are toxic and carcinogenic in nature. Since a small quantity of dye is highly visible due to its color and can cause a series of several pollution problems. Therefore, the removal of dyes from contaminated water is the major environmental concern [1]. According to recent reports, more than one million dyes are commercially available with an annual production of over 7×10^5 tons. The textile industry worldwide consumes approximately 1×10^4 tons of dyes annually and discharges nearly 100 ton/y of dyes into wastewater [2]. Wastewaters of industries like textile, paper, rubber, plastic, leather, cosmetic, food, and drug industries contain dyes and pigments which are hazardous and can cause allergic dermatitis, skin irritation, cancer, and mutation in living organisms [3]. Synthetic dyes have severe effects on the environment as well as living beings. Many dyes are toxic and carcinogenic in nature [4]. Along with these harmful properties, most dyes are inert and non-biodegradable [5]. The importance of the potential pollution of dyes and their intermediates has been incited with the toxic nature of many dyes, different mutagenic

* Corresponding author.

effects, skin diseases and skin irritation, and allergies. Moreover, they are dangerous because their microbial degradation compounds, such as benzidine or other aromatic compounds have a carcinogenic effect [6].

Reactive Yellow HE4G dye (Fig. 1), is widely used by industries. The division of azo dyes are done based on the existence of azo bonds (–N=N–) (mono azo, diazo, triazo, etc.) in the molecule [7]. Azo dyes due to their resistance to the effect of oxidation agents and light cannot be entirely treated by conventional methods of anaerobic digestion [8]. Therefore, considered necessary to develop an easy, efficient, and economic process for the removal of the hazardous dye, HE4G dyes. The present paper is an attempt to eradicate HE4G dyes using hen feather as adsorbent [9].

Adsorption is one of the best and simple techniques for the removal of toxic and noxious impurities in comparison to other conventional protocols like chemical coagulation, ion exchange, electrolysis, biological treatments is related to advantages viz. lower waste, higher efficiency, and simple and mild operational conditions. Adsorption techniques also have more efficiency in the removal of pollutants which are highly stable in the process through economically feasible mild pathways [4,10,11]. Thus, the extensive utilization of adsorption techniques for the deletion of numerous chemicals from aqueous solutions seems logical [12]. For deletion of dye pollutants, nanomaterial's based adsorbents are highly proposed [13]. The physical and chemical properties of the adsorbent are determinative in the efficient applicability of an adsorption process. Among the essential properties of an adsorbent, high adsorption capacity, recoverability, and availability at economical cost are mentionable. Nowadays, diverse potential adsorbents have been used for the deletion of specified organics from water samples. From this perspective, an extensive survey was conducted on magnetic nanoparticles (MNPs) as novel adsorbents with high adsorption capacity, large surface area, and small diffusion resistance. As an instance, for dissociation of chemical species like environmental pollutants, metals, dyes, and gases, MNPs were used [14–16].

Lead sulfide (PbS) refers to a semiconducting material of an IV–VI group with a narrow bandgap [17]. PbSnano crystals, in the past, have thoroughly been scrutinized due to the strong quantum confinement of both electrons and holes [18]. PbS nanopowders can be synthesized through a wide variety of physical and chemical methods [19]. Recently, there has been a growing interest in the investigation of the dopant behavior in the structural and optical properties of PbS nanocrystal in both powder and thin-film forms [20]. More specifically, PbS doped with various metal ions have attracted major attention owing to its controllable physical behavior [21], investigated the paramagnetic behavior of PbS down to 5 K by substitutional doping of magnetic atoms Mn. It is worth noticing the fact that artificial materials particularly metamaterials [22,23] have attracted great interest because of their superior potential application. Due to their extraordinary properties such as a negative index of refraction and electromagnetic cloak, studies on metamaterials is still in great demand [24].

In this article, with the help of the precipitation method, pure Mn-doped PbS (PbS:Mn) nanoparticles were synthesized. Then, characterization of synthesized nanopowders

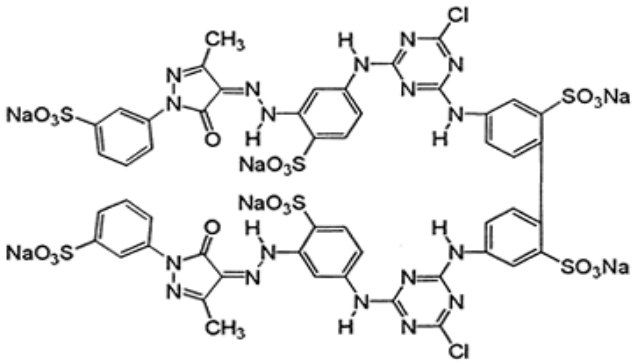

Fig. 1. Chemical structure of yellow HE-4G dye, $C_{50}H_{32}Cl_2N_{18}Na_6O_{20}S_6$, and molecular weight: 1,606.14 g/L.

was done using Brunauer–Emmett–Teller theory (BET), Fourier transform infrared (FT-IR) spectra, X-ray diffraction (XRD), and scanning electron microscopy (SEM). Cubic structure and single-phase nature of pure and Mn-doped PbS have been revealed in XRD studies. For the deletion of HE4G dyes from aqueous solutions, this adsorbent was employed. Accordingly, for the deletion of HE4G dyes from wastewater, we had a good reason to provide and utilize Pure Mn-doped PbS (PbS:Mn) nanoparticles as inexpensive, safe, and environmentally friendly adsorbents. Therefore, experimental conditions The effect of (pH of the solution, adsorbent dosage (dose), initial HE4G dye concentration (C_0) contact time (t_c), and temperature (T)) on the removal percentage (Ad%) of HE4G dye onto Mn-doped PbS (PbS:Mn) nanoparticles were scrutinized and optimized. To fit the experimental equilibrium data, different isotherm models of Langmuir, Freundlich, and Dubinin–Radushkevich were applied [25]. The applicability and usefulness of the Langmuir model were proven by the obtained outcomes. Kinetic models, such as pseudo-first-order, pseudo-second-order diffusion, and Elovich models indicated that the pseudo-second-order model controls the kinetics of the adsorption process. The effectiveness of pure Mn-doped PbS (PbS:Mn) nanoparticles in deleting HE4G dyes from wastewater was confirmed.

2. Experimental

2.1. Preparation of stock solution

Reactive Yellow HE4G dye (Jasynth in India provided) $Pb(NO_3)_2$, thiourea $[SC(NH_2)_2]$, $Mn(OAc)_2$ $4H_2O$, sodium hydroxide, hydrochloric acid. They were supplied from Merck (Darmstadt, Germany). All used chemicals were of reagent grade and utilized without further purification. For the pH adjustment, hydrochloric acid (HCl) and sodium hydroxide (NaOH) were applied.

2.2. Reagents and instruments

UV-visible spectra, dyes concentrations were determined and their measurements were done using a Maya Pro 180 spectrophotometer (Shimadzu Company, Japan). FT-IR spectra were recorded on a PerkinElmer (FT-IR spectrum BX, Germany). The structure and phase evaluation of prepared

samples was carried out by using Philips X pert MPD, and X-ray diffractometer with CuKα radiation at beam acceleration conditions of 40 kV/35 mA. The morphology of samples was studied by scanning electron microscopy (SEM: KYKY-EM 3200, Hitachi Company, China). The pH/ion meter (model-728, Metrohm Company, Switzerland, Swiss) was used for the pH measurements. Laboratory glassware was kept overnight in 10% nitric acid solution.

2.3. Preparation of Mn-doped PbS (PbS:Mn) nanoparticles

The synthesis of pure and Mn-doped PbS (PbS:Mn) nanoparticles was executed at ambient temperature by the precipitation method. In this process for preparing pure PbS first 0.01 mol of $Pb(NO_3)_2$ was dissolved in 25 mL of deionized water (DW) for 15 min under consecutive stirring. The XRD patterns of $PbS_{(1-x)}Mn_x$ nanoparticles (x = 0%, 5%, 10%, and 15%). The nanoparticle PbS was synthesized in the reactive solution prepared using lead nitrate [$Pb(NO_3)_2$] and thiourea [$SC(NH_2)_2$] with the concentration of 0.06 and 0.25 M. The NaOH pellets were used as a base medium and its concentration was set to 0.6 M. 150 mL of all the above solutions were prepared separately, using distilled water as a solvent and mixed together in a beaker. 0.1 M of EDTA was added into the solution as a complexing agent, which can easily bind the metal ions. The reactive vessel with the solution was immersed into an oil bath maintained at 80°C:

$$Pb(NO_3)_2 + 2NaOH \rightarrow Pb(OH)_2 + 2NaNO_3 \quad (A)$$

$$Pb(OH)_2 + 2NaNO_3 \rightarrow Na_4Pb(OH)_6 \quad (B)$$

$$Na_4Pb(OH)_6 \rightarrow 4Na^+ + HPbO_2^- + 3OH^- + H_2O \quad (C)$$

In the alkaline medium, the thiourea decomposes and releases S_2 ions. Pb_2S ions precipitate from the solution leading to the formation of PbS [26]:

$$SC(NH_2)_2 + OH^- \rightarrow CH_2N_2 + H_2O + SH^- \quad (D)$$

$$HPbO_2^- + SH^- \rightarrow PbS + H_2O + SH^- \quad (E)$$

Three samples of Mn-doped PbS nanoparticles were provided likewise through implementing change in the concentration of $Mn(OAc)_2$ $4H_2O$ 15 mol %. Typically Mn-doped PbS nanoparticles were synthesized by dissolving a specific amount of $Mn(OAc)_2{\cdot}4H_2O$ in 25 mL DW. The stirring continued vigorously for 15 min. Continuous washing of the obtained mixture and oven drying of it led to the synthesis of Mn-doped PbS nanoparticles [27].

2.4. Adsorption of HE4G dye onto Mn-doped PbS (PbS:Mn) nanoparticles

In the company, a batch process utilizing Mn-doped PbS (PbS:Mn) nanoparticles was used for binary sorption of HE4G dye. The evaluation of the thermodynamic properties of the adsorption process was performed by adding 0.1 g of pure Mn-doped PbS (PbS:Mn) nanoparticles into 50 mL initial HE4G dye concentration ranging from 10 mg/L in each experiment. For 15 min and at 25°C, each solution was shaken uninterruptedly. The HE4G dye concentration was estimated after the solution equilibrium and desorption outcomes were obtained in the present work.

2.5. Batch adsorption dye adsorption

Generally, the batch method is currently used in adsorption studies. This method includes the following steps: (I) selecting an adequate solution of adsorbate with a known initial concentration in a suitable (50.0 mL, C_0 = 10.0 mg/L), (II) adding an adequate dosage of adsorbent to the previous solution (0.10 g), (III) adjusting pH and temperature on desirable values (2.0°C and 25.0°C), (IV) stirring the resultant mixture in step (III) for a suitable contact time (15.0 min), (V) separating the solid phase from the solution phase under the equilibrium state by an effective technique (centrifuge), (VI) the HE4G dye concentration in the solution was measured using a double beam UV-vis spectrophotometer (Maya Pro 180 Shimadzu Company, Japan), set at wavelengths 675 nm for HE4G dye, and (VII) evaluating the removal percentage (Ad%) and adsorption capacity of the adsorbent (q_e) from the following equations:

$$\%\text{Ad dye} = \frac{\left(C_0 - C_t\right)}{C_0} \times 100 \quad (1)$$

where C_0 and C_t refer to the initial concentration of dye (mg/L) and the concentration of dye at any time (mg/L), respectively.

$$q_e = \frac{\left(C_0 - C_e\right)V}{W} \quad (2)$$

In the above equation, q_e, C_0, C_e, V, and W refer to adsorption capacity (mg/g), the primary concentrations of dye (mg/mL), the equilibrium concentrations of dye (mg/mL), the volume of the aqueous phase (mL), and the weight of the adsorbent (g), respectively.

3. Results and discussion

3.1. Characterization of adsorbent

3.1.1. BET analysis of Mn-doped PbS (PbS:Mn) nanoparticles

Bulk density, surface area, and loss of mass on ignition are shown in Table 1. The bulk density affects the rate of adsorption of HE4G dye solution by Mn-doped PbS (PbS:Mn) nanoparticles. In the present study, the bulk density was less than 1.0 indicating that the activated carbon materials are in fine nature and hence enhanced the adsorption of HE4G dye from aqueous solution [28]. The moisture content (0.5%) was determined, even though it does not affect the adsorption power, dilutes the adsorbents, and therefore necessitates the use of the additional weight of adsorbents to provide the required weight. The surface area of Mn-doped PbS (PbS:Mn) nanoparticles in the present research study were 250 m^2/g and are higher than a low-cost agro-based adsorbent such as Mn-doped PbS (PbS:Mn) nanoparticles (45.231 m^2/g and 1.34×10^{-2} cm^3/g).

3.1.2. FTIR analysis

In Fig. 2, FTIR spectra for Mn-doped PbS nanoparticles (x = 15%) are exhibited. By FTIR analysis almost detecting the vibrational frequencies for stretching bonds in PbS molecule is impossible which is a good indication for the fact that PbS doesn't display any definite absorption signals in the range 400–4,000 cm^{-1}. Because of the presence of the hydroxyl group in the compound, the existed vibration modes at 3,437 cm^{-1} is assignable to the O–H broad absorption mode. Attributed to the C–H tensile vibration 2,935 cm^{-1} of the methylene group acetate in $Mn(OAc)_2{\cdot}4H_2O$ for synthesis of Mn-doped PbS nanoparticles. The wide absorption near 1,300–1,000 cm^{-1} is a good indication of the presence of the C–O bond. The absorption band at 1,003 and 641 cm^{-1} is due to the Mn–O bending in the molecules adsorbed into the surface. The O–H bending vibration from the water molecules adsorbed into the surface resulted in the absorption band at 1,645 cm^{-1}. In addition indefinite points might prove that no significant difference existed between the FTIR spectra of pure PbS nanoparticled and Mn-doped PbS nanoparticles [29].

3.1.3. XRD analysis

Different X-ray emission peaks are Mn-doped PbS nanoparticles, the adsorption of HE4G dye and based in (Fig. 3), show peaks at 2θ = 25.8°, 30.5°, 42.8°, 51.2°, 53.7°, 62.4°, 68.3°, 71.5°, and 79.2° belong to the lattice planes of (111), (200), (220), (311), (222), (400), (331), (420), and (422) planes pertain to the pure cubic phase of PbS [29,30]. Obviously, the perfect crystalline nature of the material was proven after functionalizing with Mn-doped PbS nanoparticles however the great intensity of the signal at 25.8 (111) and 30.5 (200) confirmed that there has been a slight amount of material in an amorphous state. The perfect synthesis of Mn-doped PbS nanoparticles is obvious through looking at the XRD pattern of the crystal.

Table 1
Characteristics of the Mn-doped PbS (PbS:Mn) nanoparticles

Parameter	Value
pH	7.0
Moisture (%)	0.5
Bulk density (g/mL)	0.45
Surface area (m^2/g)	250
Particle size range (μm)	45–250
Loss of mass on ignition	0.6235

3.1.4. Surface morphology

The morphological properties of the investigated samples by SEM are exhibited in Figs. 4a and b. As demonstrated in Fig. 4c, the evenness, homogeneity, orderliness, and approximate uniformity of $Pb_{1-x}Mn_xS$ nanoparticles (x = 15%) (even in size distribution) was observed. After surface modification, it has been seen that the particles were mostly spherical with various size distribution as they form agglomerates. From the particle size distribution, we obtain the average particle size in the range of 37–44 nm very close to those determined by XRD analysis [31].

3.1.5. Thermal analysis

Thermal gravimetric analysis (TGA) of synthesized Mn-doped PbS nanoparticles was performed from 200°C

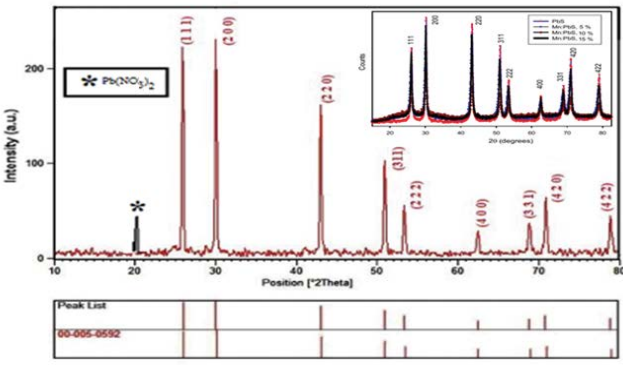

Fig. 3. XRD patterns of $PbS_{1-x}Mn_x$ nanoparticles (x = 0%, 5%, 10%, and 15%).

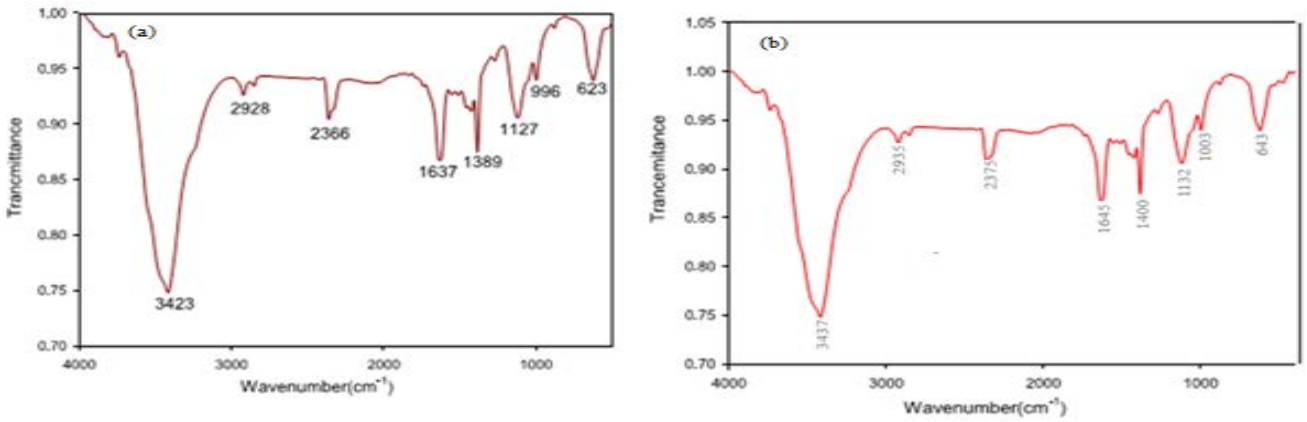

Fig. 2. FTIR spectra of Mn-doped PbS nanoparticles (a) before and (b) after HE4G dye.

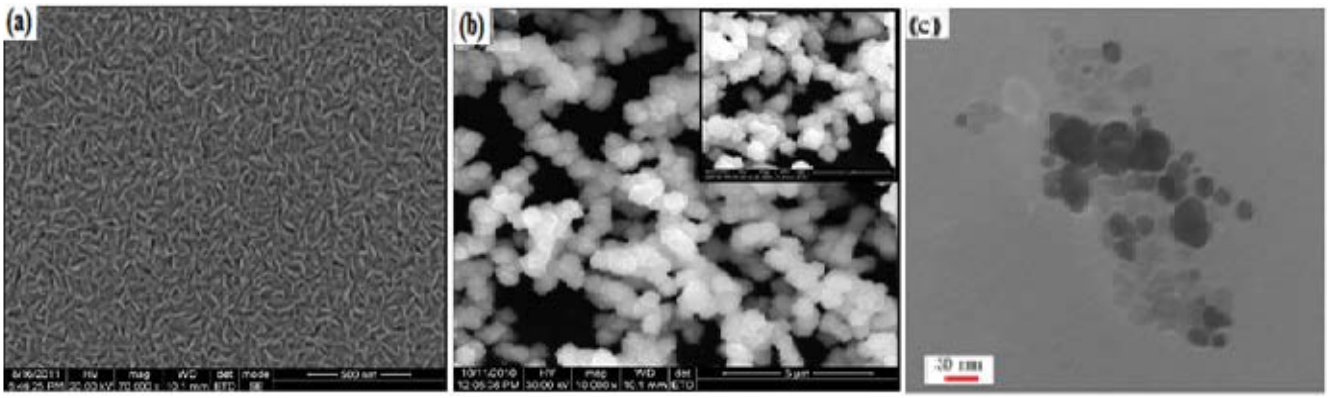

Fig. 4. SEM image (a) pure PbS nanoparticles, (b) Mn-doped PbS nanoparticles, and (c) TEM of the prepared 15 mol% Mn-doped PbS nanoparticles.

to 1,000°C. The TGA curve of Mn-doped PbS nanoparticles are exhibited in (Fig. 5a), which in that, a single stage of weight loss is revealed. Also (Fig. 5b), demonstrates the resultant differential thermal analysis (DTA) traces of synthesized Mn-doped PbS nanoparticles. However, an endothermic signal with the highest value of 762°C is discerned. The first pointed endothermic signal emerging in the DTA trace is ascribed to its melting. The point 1,113°C is considered the melting point of the bulk Mn-doped PbS nanoparticles material [31]. Because of the reduction in the particle size of synthesized Mn-doped PbS nanoparticles, its melting point is considerably shifted toward a lower value.

3.2. Impact of pH on the adsorption

The impact of pH value in the adsorption process is considerable. The deletion of HE4G dye as a function of pH by varied sorbent is shown in (Fig. 6). To control optimum pH for the highest deletion of HE4G dye, the measurement of equilibrium adsorption of HE4G dye was done at varied pH levels from 2.0 to 9.0 through adjusting the initial HE4G dye concentrations at 10 mg/L and the summary of the obtained outcomes are displayed [32]. The maximum adsorption percent was observed at pH 2.0. So, the remaining all adsorption experiments were carried out at this pH value. This amount for pure PbS was 78.3, for PbS/Mn-5% was 80.9, for PbS/Mn-10% was 84.2 and for PbS/Mn-15% was 87.4% showed in Table 2. The adsorption mechanism may be considered as physicochemical interaction between adsorbent/adsorbate pair [33]. At a highly acidic pH, the active sites of the adsorbent would be occupied by H^+_{aq} ions, which results in lower uptake of HE4G dye onto Mn-doped PbS (PbS:Mn) nanoparticles. In turn, the adsorbent surface becomes considerably negatively charged as the pH solution increases from 2.0 to higher values which cause in lower up taking of HE4G dye Mn-doped PbS (PbS:Mn) nanoparticles, so the pH = 2.0 is the optimum value in the HE4G dye adsorption onto the Mn-doped PbS (PbS:Mn) nanoparticles adsorbent.

3.3. Impact of the contact time

The contact time is an effective factor which affects considerably Ad%. Indeed, for maintaining the adsorbent/adsorbate equilibrium, it should enough prolong the contact time for setting up the equilibrium between adsorbent and adsorbate (Fig. 7), indicates the effect of contact time on sorption of HE4G dye by Mn-doped PbS (PbS:Mn) nanoparticles. The net result of contact time on sorption of HE4G dye using synthesized PbS, PbS/Mn-5%, PbS/Mn-10%, and PbS/Mn-15%nanoparticles is exhibited in Fig. 7. A little change in sorption rate was

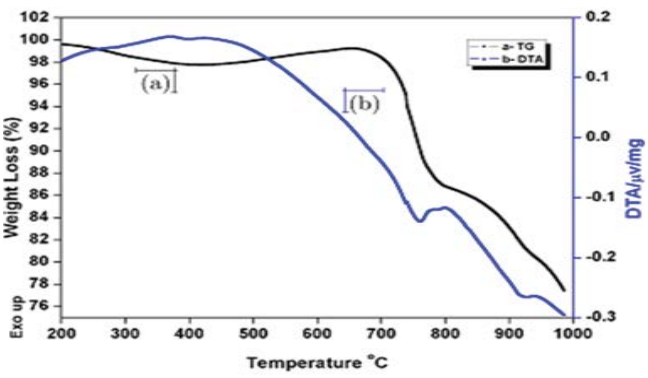

Fig. 5. (a) TGA curves (color online) and (b) DTA curves of synthesized Mn-doped PbS nanoparticles.

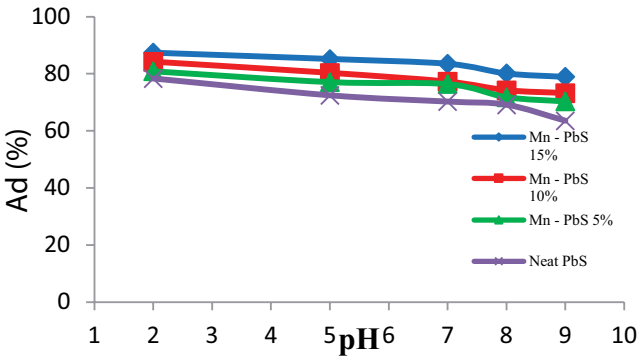

Fig. 6. Impact of pH on HE4G dye deletion (HE4G dye concentration = 10 mg/L; adsorbent dose = 0.1 g/L; contact time = 15 min; stirring speed = 180 rpm; and temperature = 25°C).

Table 2
Adsorption quality and distribution coefficient parameters for Yellow HE4G dye solution (10 mg/L, pH = 2), for pure PbS, PbS/Mn-5%, PbS/Mn-10%, and PbS/Mn-15% nanoparticles

	Yellow HE4G dye (mg/L)				
Sorbent	Initial (C_i)	Final (C_e)	Removal efficiency (%)	K_d (mL/g) × 10^3	q_{max} (mg/g)
PbS	10	2.17	78.3	3.132	6.796
PbS/Mn-5%	10	1.91	80.9	3.236	6.181
PbS/Mn-10%	10	1.58	84.2	3.368	5.321
PbS/Mn-15%	10	1.26	87.4	3.496	4.405

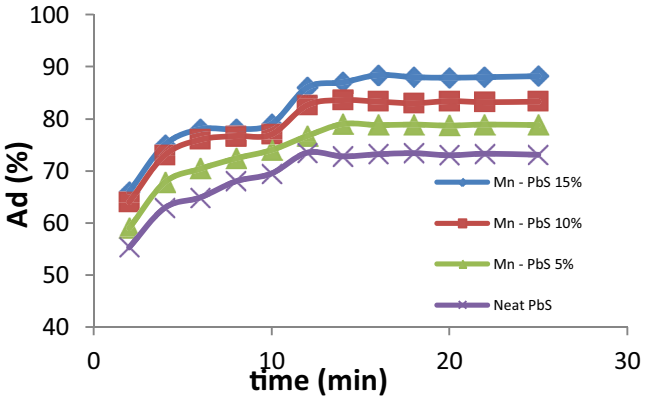

Fig. 7. Net result of time on HE4G dye deletion (HE4G dye concentration = 10 mg/L; pH = 2.0; contact dose adsorbent = 0.1 g; stirring speed = 180 rpm; temperature = 25°C).

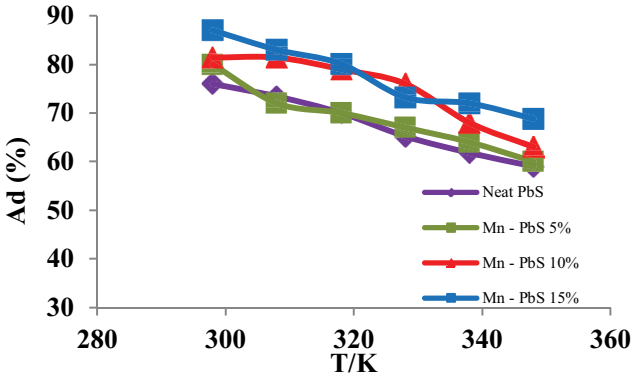

Fig. 8. Net result of temperature on HE4G dye deletion (HE4G dye concentration = 10 mg/L; adsorbent dose = 0.1 g/L; pH = 2.0; contact time = 15 min; stirring speed = 180 rpm).

observed at 16 min for pure PbS nanoparticles, at 14 min for PbS/Mn-5% and PbS/Mn-10%, and at 12 min for PbS/Mn-15%. The sorption rate leveled off little by little until when no considerable increase was observed in the HE4G dye adsorption and the deletion finally reached equilibrium [34]. Therefore, the maximum of removal percentages at contact time 16, 14, 14, and 12 min for pure PbS, PbS/Mn-5%, PbS/Mn-10%, and PbS/Mn-15% nanoparticles respectively, is 88.4%, 83.6%, 79.0%, and 73.5%.

3.4. Impact of temperature

The net result of temperature on the adsorption of HE4G dye is shown in (Fig. 8). Based on the obtained results, a gradual boost in the removal percentage for pure PbS/Mn-15% nanoparticles from 68.8% to 87.0%, for pure PbS/Mn-10% nanoparticles from 63.0% to 81.4%, for pure PbS/Mn-5% nanoparticles from 60.0% to 80.0% and for pure PbS nanoparticles from 59.0% to 76.0% was observed. To study the effect of temperature on the adsorption percent of HE4G dye into sorbent, the experiments were performed at temperatures range of 298.0–328.0 K (Fig. 8) shows the results. Since adsorbent is porous in nature and possibilities of diffusion of adsorbate cannot be ruled out, therefore, increase in the sorption with the rise of temperature may be diffusion controlled which is an exothermic process, the rise of temperatures favors the adsorbate transport with in the pores of adsorbent [35].

3.5. Adsorption isotherms

Considering the variation of equilibrium adsorption capacities in terms of the equilibrium concentration (C_e) of the adsorbate, under the optimum values of other parameters, we can examine some suitable isotherms for representing the respect experimental data [36,37]. Adsorption equilibrium isotherm is designed based on mathematical relation of the amount of adsorbed target per gram of adsorbent (q_e (mg/g)) to the equilibrium non-adsorbed amount of dyes in solution (C_e (mg/L) at fixed temperature [38]. To investigate the adsorption isotherm of adsorption, three models, Langmuir adsorption isotherm, Freundlich adsorption isotherm, and Dubinin–Radushkevich (D–R) isotherms were used.

- Langmuir adsorption isotherm: in this model, there is no interaction among adsorbed molecules and the adsorption process happens on homogeneous surfaces. The Langmuir model showed in Eq. (3) [39]:

$$\frac{C_e}{q_e} = \frac{1}{K_L q_{max}} + \frac{C_e}{q_{max}} \tag{3}$$

where C_e (mg/L), q_e (mg/g), and q_{max} (mg/g) signify the equilibrium concentration, the adsorption capacity, and the maximum adsorption capacity of the adsorbents in the aqueous solution, respectively. K_L is a constant

related to the binding energy of the sorption system (L/mg) (Fig. 9a).

- Freundlich adsorption isotherm: This model can be explained the multilayer adsorption of adsorbate onto a heterogeneous surface of an adsorbent. The linear form of Freundlich isotherm model expression is given as:

$$\ln q_e = \ln K_F + \left(\frac{1}{n}\right)\ln C_e \tag{4}$$

That K_F (the adsorption capacity) and n (intensity of a given adsorbent) are the Freundlich isotherm constant (Fig. 9b).

The values of the constants in both models are obtained from the slope and the position (Figs. 9a and b and Table 3), shows the results of the fit and of the constants of both models for HE4G dye. The values of n for pure PbS, PbS/Mn-5%, PbS/Mn-10%, and PbS/Mn-15% nanoparticles were 8.064, 3.534, 2.203, and 1.792, respectively. The values between 1 and 10 for n in the adsorption process are favorable. All the correlation coefficients and parameters obtained for the isotherm models from (Table 3), reveal that the Langmuir isotherm is the best model to demonstrate the adsorption of HE4G dye for pure PbS, PbS/Mn-5%, PbS/Mn-10%, and PbS/Mn-15% nanoparticles adsorbent.

- Dubinin–Radushkevich (D–R) isotherms: For investigated the nature of adsorption, this model is used. The linear form of this model expressed by the following equation:

$$\ln q_e = \ln q_m - \beta\varepsilon^2 \tag{5}$$

where β is the activity coefficient related to mean sorption energy (mol²/kJ²), and ε is the Polanyi potential, that can be calculated from the bellow equation:

$$\varepsilon = RT\ln\left(1+\frac{1}{C_e}\right) \tag{6}$$

where R and T are the ideal gas constant (8.3145 J/mol K) and absolute temperature (K), respectively (Fig. 9c). E_a is the free energy change of adsorption (kJ/mol), which required transferring 1 mol of ions from solution to the adsorbent surface, which can be calculated from the Eq. (7) [40]:

$$E_a = \frac{1}{(-2\beta)^{1/2}} \tag{7}$$

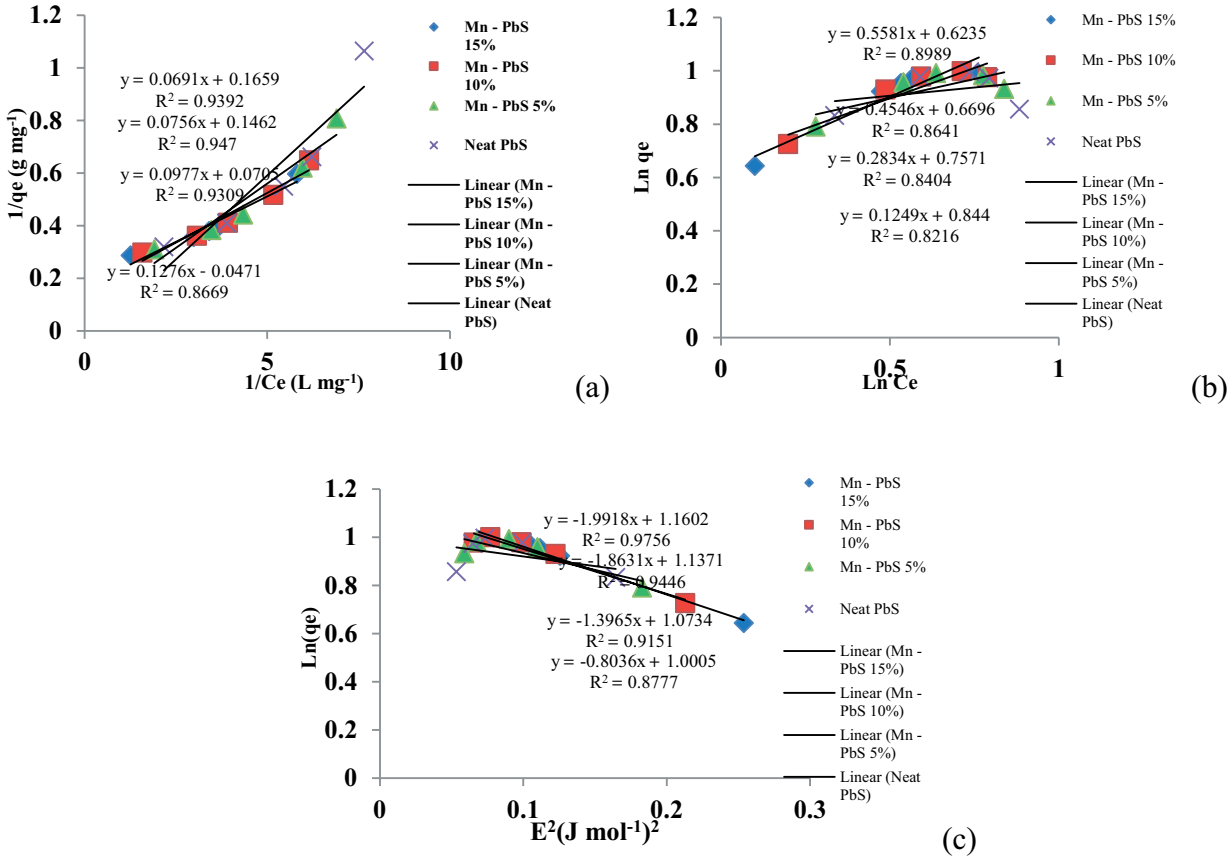

Fig. 9. (a) Langmuir, (b) Freundlich, (c) Dubinin–Radushkevich isotherm for the adsorption of HE4G dye onto synthesized pure sorbent PbS, PbS/Mn-5%, PbS/Mn-10%, and PbS/Mn-15% nanoparticles (HE4G dye concentration = 10 mg/L; adsorbent dose = 0.1 g/L; pH = 2.0; contact time = 15 min; stirring speed = 180 rpm; temperature = 25°C).

Table 3
Varied isotherm constants and correlation coefficients computed for the adsorption of HE4G dye onto synthesized pure sorbent PbS, PbS/Mn-5%, PbS/Mn-10%, and PbS/Mn-15% nanoparticles (HE4G dye concentration = 10 mg/L; adsorbent dose = 0.1 g/L; pH = 2.0; contact time = 15 min; stirring speed = 180 rpm; temperature = 25°C)

Isotherm	Parameters	Value of parameters for PbS/Mn-15%	Value of parameters for PbS/Mn-10%	Value of parameters for PbS/Mn-5%	Value of parameters for pure PbS
	q_m (mg/g)	144.93	133.33	103.09	78.74
Langmuir	K_L (L/mg)	0.418	0.514	1.386	2.702
	R^2	0.939	0.947	0.930	0.866
	n	1.792	2.203	3.534	8.064
Freundlich	K_F (mg)$^{1-n}$ L^n/g	4.198	4.667	5.715	6.982
	R^2	0.898	0.864	0.840	0.821
	q_m (mg/g)	120.2	100.8	60.5	41.8
Dubinin–Radushkevich	$B_D \times 10^{-7}$ /(mol^2 kJ^2)	7.5	7.0	6.6	6.0
(D–R)	E_D (kJ/mol)	–903.0	–817.12	–770.1	–700.0
	R^2	0.975	0.944	0.915	0.877

In this model, E_a > 8 kJ/mol in this model is a good indication that the mechanism of adsorption is physical while 8 < E_a < 20 kJ/mol is a good indication of chemical ion exchange and E_a < 20 kJ/mol well indicate that the mechanism of HE4G dye adsorption is chemical [41]. The *E*-value of –700.0 is for pure PbS, –770.1 for PbS/Mn-5% –817.12 for PbS/Mn-10%, and –903.0 for PbS/Mn-15% nanoparticles. Therefore, it is suggested that HE4G dye adsorption for pure PbS, PbS:Mn-5%, PbS/Mn-10%, and PbS/Mn-15% nanoparticles adsorbent is physical.

3.6. Adsorption kinetic investigations

Adsorption of a solute by a solid in an aqueous solution through complex stages [42], is strongly influenced by several parameters related to the state of the solid (generally with the very heterogeneous reactive surface) and to physico-chemical conditions under which the adsorption occurs. The rate of dyes adsorption onto the adsorbent has been fitted to traditional models like pseudo-first-order and pseudo-second-order models and so on. The Lagergren pseudo-first-order model can describe some of the adsorption kinetic data equation and it:

$$\frac{dq_t}{dt} = k_1\left(q_e - q_t\right) \tag{8}$$

where q_e and dq_t (mg/g) are the adsorption capacities at equilibrium and at time *t*, respectively. k_1 is the rate constant of the pseudo-first-order adsorption (min^{-1}). The integrated form of Eq. (8) is:

$$\log\left(q_e - q_t\right) = \log q_m - \left(\frac{k_1}{2.303}\right)t \tag{9}$$

Thus, the slope of $\log(q_e - q_t)$ vs. *t* is equal to k_1/2.303 and the inception is equal to $\log q_m$ [43].

Pseudo-second-order model is represented as:

$$\frac{dq_t}{dt} = k_2\left(q_e - q_t\right)^2 \tag{10}$$

$$\frac{t}{q_t} = \frac{1}{k_2 q_e^2} + \frac{t}{q_e} \tag{11}$$

The intra-particle-diffusion model has based on the hypothesis that the mechanism of dye removal onto a sorbent material occurs through four steps: (1) bulk diffusion, which is the migration of dye molecules from the bulk solution to the surface of the adsorbent, and (2) formation the film diffusion, which is the diffusion of dye molecules through the boundary layer to the surface of the adsorbent, and (3) dye adsorption on the active sites of the surface of the adsorbent, and (4) intraparticle diffusion, which is the migration of dye molecules to the interior pore structure of adsorbent. The adsorption process is a diffusive mass transfer process where the rate can be expressed in terms of the square root of time (*t*). The intra-particle-diffusion model can be represented as:

$$q_t = k_i t^{0.5} + I \tag{12}$$

where k_i is the intraparticle diffusion rate constant (mg/g min$^{0.5}$) and *I* is the effect of boundary layer thickness. The obtained kinetic data for HE4G dye adsorption onto Mn-doped PbS (PbS:Mn) nanoparticles and adsorbent were examined with the above-mentioned kinetic model's Figs. 10a–c. As we can see from Fig. 10, the list in Table 4, demonstrates the correlation coefficient (R^2) values of the three kinetic models and other calculated, connected kinetic parameters. The calculated values of the correlation coefficient (R^2) proved the perfect matching of the pseudo-second-order model fitted better the kinetic data of this work than others (R^2 = 0.9999) when compared to other models for interpretation of adsorption mechanism of HE4G dye for pure PbS, PbS/Mn-5%, PbS/Mn-10%, and PbS/Mn-15% nanoparticles [44,45].

3.7. Adsorption thermodynamics

Generally, adsorption thermodynamics is related to the definition of a conditional equilibrium constant (K_c) as:

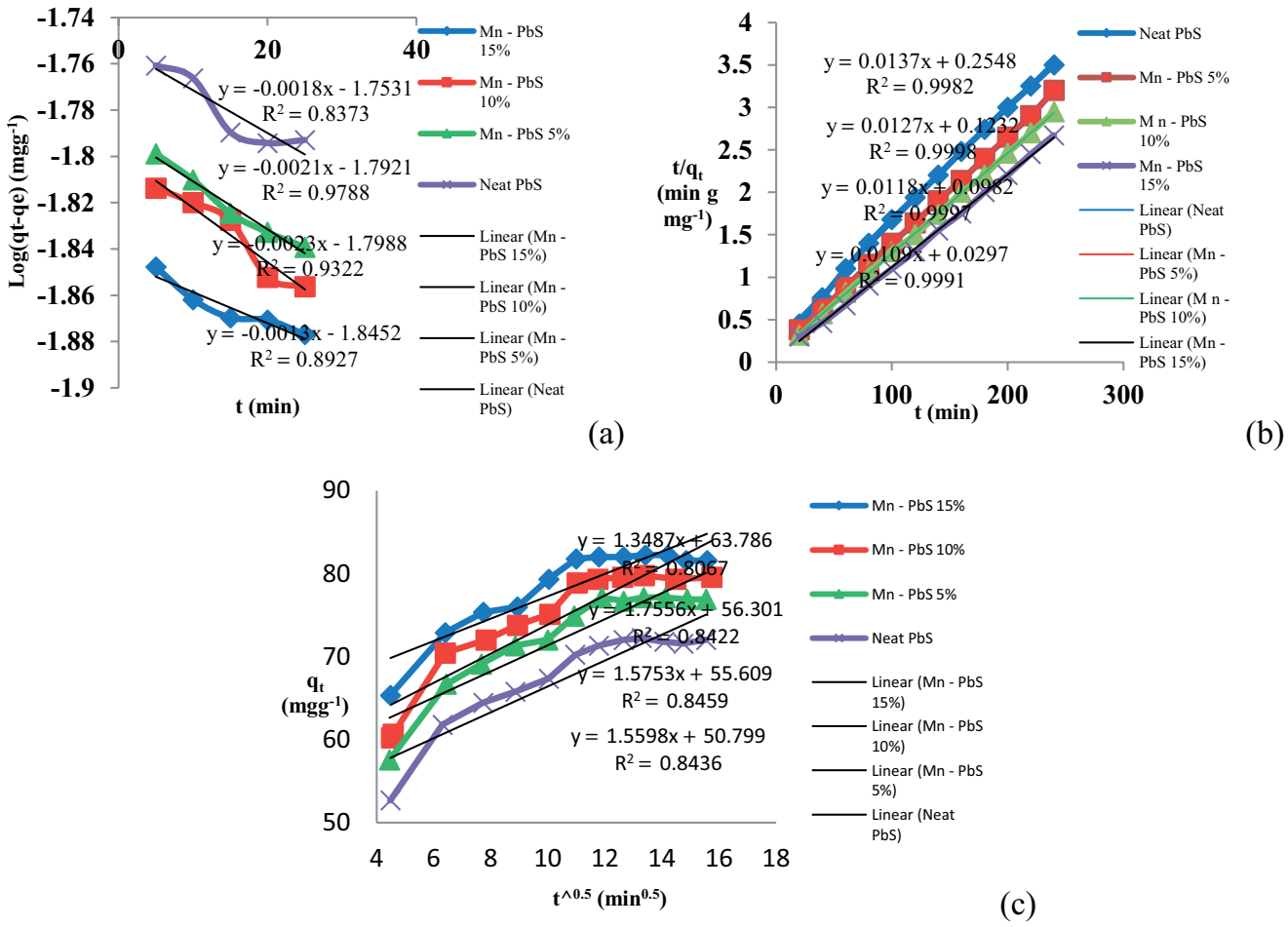

Fig. 10. (a) Pseudo-first-order model, (b) pseudo-second-order model, (c) Elovich model for adsorption of HE4G dye onto synthesized pure sorbent PbS, PbS/Mn-5%, PbS/Mn-10%, and PbS/Mn-15% nanoparticles (HE4G dye concentration = 10 mg/L; adsorbent dose = 0.1 g/L; pH = 2.0; contact time = 15 min; stirring speed = 180 rpm; temperature = 25°C).

Table 4
Juxtaposition of the kinetic parameters for adsorption of HE4G dye onto synthesized pure sorbent PbS, PbS/Mn-5%, PbS/Mn-10%, and PbS/Mn-15% nanoparticles (HE4G dye concentration = 10 mg/L; adsorbent dose = 0.1 g/L; pH = 2.0; contact time = 15 min; stirring speed = 180 rpm; temperature = 25°C)

Model	Parameters	Value of parameters for PbS/Mn-15%	Value of parameters for PbS/Mn-10%	Value of parameters for PbS/Mn-5%	Value of parameters for PbS
Pseudo-first-order kinetic $\log(q_e - q_t) = \log(q_e) - \left(\frac{k_1}{2.303}\right)t$	$q_{e,cal}$ (mg/g)	17.7	17.5	15.7	16.9
	K_1 (min^{-1})	0.034	0.038	0.036	0.03
	R^2	0.8967	0.9322	0.9788	0.8373
Pseudo-second-order kinetic $\frac{t}{q_t} = \frac{1}{k_2 q_e^2} + \left(\frac{1}{q_e}\right)t$	$q_{e,cal}$ (mg/g)	55.01	48.10	39.26	30.18
	K_2 (g/mg min)	0.082	0.057	0.062	0.051
	R^2	0.9999	0.9997	0.9998	0.9982
Elovich $q_t = \frac{1}{\beta}\ln(\alpha\beta) + \frac{1}{\beta}\ln(t)$	β (mg/g min)	0.0281	0.0263	0.0288	0.0414
	α (g/mg)	54.334	54.233	62.998	75.137
	R^2	0.8436	0.8459	0.8422	0.8067

$$K_c = \frac{q_e}{C_e} \tag{13}$$

Therefore, upon determining K_c at a sufficient number of temperatures, then concluding the thermodynamic functions of the adsorption process is quite straight forward. Because:

$$\Delta G^\circ_{ad} = -RT \ln K_c \tag{14}$$

$$\ln K_c = \frac{\Delta S^\circ_{ad}}{R} - \frac{\Delta H^\circ_{ad}}{RT} \tag{15}$$

$$\ln\left(\frac{K_{c(2)}}{K_{c(1)}}\right) = -\frac{\Delta H^\circ_{ad}}{R}\left(\frac{1}{T_2} - \frac{1}{T_1}\right) \tag{16}$$

where ΔG°_{ad}, ΔH°_{ad}, and ΔS°_{ad} represent respectively the standard change of Gibbs free energy, enthalpy, and entropy associated to the respect adsorption process. T is the temperature in Kelvin. In this research, the values of K_c were calculated at 298.0, 308.0, 318.0, 328.0, 338.0, and 348.0 K temperatures. The plot of $\ln K_c$ vs. $(1/T)$ is shown in (Fig. 11), from which the values ΔH°_{ad} and ΔS°_{ad} can be deduced (Table 5). As we can see from Table 5, the values of K_c are greater than 1 at any used temperature, so, ΔG°_{ad} upon Eq. (14) should be negative indicating that the studied adsorption process is spontaneous in the range of used temperature, $\Delta H^\circ_{ad} < 0$ indicates that the studies adsorption is exothermic. Based on the magnitude of ΔH°_{ad}, we can say that the mentioned adsorption should be physisorption one and van der walls interactions are responsible for adsorption taking place. $\Delta S^\circ_{ad} < 0$ indicates a decrease in randomness that occurs during HE4G dye adsorption onto Mn-doped PbS (PbS:Mn) nanoparticles,

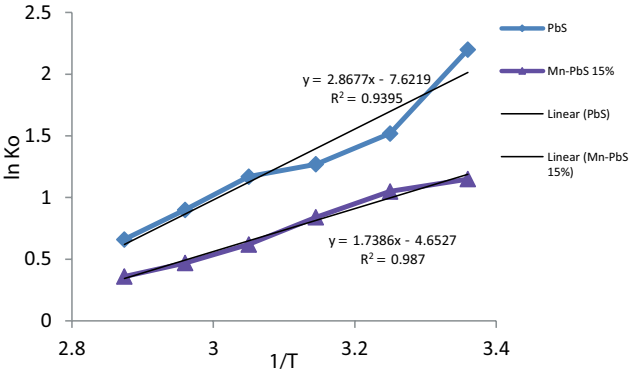

Fig. 11. Plot of $\ln K_c$ vs. $1/T$ for the estimation of thermodynamic parameters for the adsorption of HE4G dye onto synthesized pure sorbent PbS and PbS/Mn-15% nanoparticles (HE4G dye concentration = 10 mg/L; adsorbent dose = 0.1 g/L; pH = 2.0; contact time = 15 min; stirring speed = 180 rpm; temperature = 25°C).

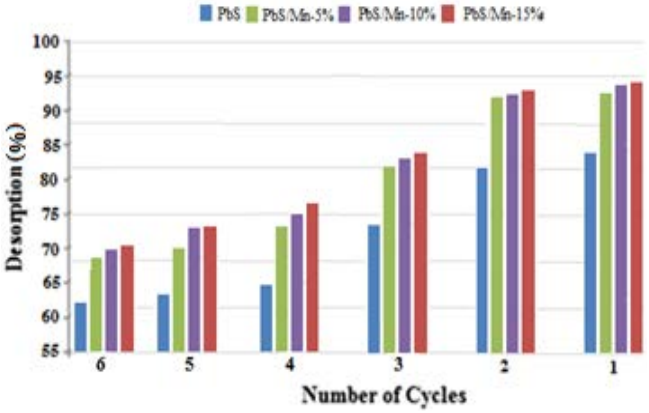

Fig. 12. Desorption of HE4G dye onto synthesized pure sorbent PbS, PbS/Mn-5%, PbS/Mn-10%, and PbS/Mn-15% nanoparticles (HE4G dye concentration = 10 mg/L; adsorbent dose = 0.1 g/L; pH = 2.0; contact time = 15 min; stirring speed = 180 rpm; temperature = 25°C).

Table 5
Thermodynamic parameters for the adsorption of HE4G dye onto synthesized pure sorbent PbS and PbS/Mn-15% nanoparticles (HE4G dye concentration = 10 mg/L; adsorbent dose = 0.1 g/L; pH = 2.0; contact time = 15 min; stirring speed = 180 rpm; temperature = 25°C)

HE4G dye (10 mg/L)	T (K)	K_c	Value of ΔS° (J/mol K)	Value of ΔH° (kJ/mol)	Value of ΔG° (kJ/mol)
Sorbent PbS	298	8.62	–63.3	–23.9	–5.337
	308	4.56			–3.885
	318	3.57			–3.365
	328	3.2			–3.172
	338	2.39			–2.448
	348	1.98			–1.976
Sorbent PbS/Mn-15% nanoparticles	298	3.17	–38.7	–14.5	–2.858
	308	2.76			–2.6
	318	2.33			–2.236
	328	1.87			–1.706
	338	1.62			–1.356
	348	1.43			–1.035

Table 6
Juxtaposition of the adsorption capacities of different adsorbents for the adsorption of removal dyes by nano sorbent

Dyes	Adsorbent	Dosage sorbent (g)	Adsorption capacity (mg/g)	References
Red 46 and basic yellow 28 dyes	Sorbent bentonite	0.4	45.87 and 40.48	[6]
Cationic dyes	ZnS:MnNPs-AC	0.025	202.43 and 191.57	[9]
Propyl paraben dye	TiO_2NPs-AC	0.027	120	[10]
Rhodamine 123 and disulfine blue dyes	Au-Fe_3O_4-NPs-AC	0.025	71.46 and 76.38	[11]
Bismark brown and thymol blue dyes	Mn-Fe_2O_4-NPs-AC	0.025	70.3 and 48.48	[16]
Naphthpl Yellow S dye	Sorbent Waktu kontak	0.2	143.72	[25]
Purpurin dye	Mn-doped Fe_2O_4 nanoparticles	0.027	60.0	[34]
HE4G dye	Mn-doped PbS (PbS:Mn) nanoparticles	0.1	144.49	Present study

which may come from the HE4G dye aggregation on the Mn-doped PbS (PbS:Mn) nanoparticles surfaces [46,47].

3.8. Recycling of the adsorbent

The ability of recovering and reusing of the adsorbent was tested in several steps of adsorption and the desorption process was done [48]. The results are shown in (Fig. 12). As shown in Fig. 12, 95/0 of HE4G dye was desorbed in the first cycle and after six cycles, there were slight changes in HE4G dye onto synthesized pure sorbent PbS, PbS/Mn-5%, PbS/Mn-10%, and PbS/Mn-15% nanoparticles desorption. So, it was concluded that the desired removal of 93% can be achieved after six cycles.

3.9. Juxtaposition of dyes onto nano sorbent batch adsorption method with other

Table 6, demonstrates the max adsorption capacities of varied adsorbents for deletion of dyes comparatively. The type and density of active sites in adsorbents that are responsible for the adsorption of metal ions from the solution result in the variation in q_{max} values.

4. Conclusion

The selection of Mn-doped PbS (PbS:Mn) nanoparticles as an efficacious adsorbent for the deletion of HE4G dye from aqueous solutions has been investigated. In the present study, the applicability of Mn-doped PbS (PbS:Mn) nanoparticles as an available, useful, and affordable for deleting HE4G dye from aqueous solutions has been confirmed. The desired values of the pH, adsorbent dosage, HE4G dye concentration, and contact time were chosen to be 2, 0.1 g, 10 mg/L, and 15 min for pure PbS, PbS/Mn-5%, PbS/Mn-10%, and PbS/Mn-15% nanoparticles, respectively. The influence of different process parameters demonstrated that the percentage of adsorption lessened with the boost in initial HE4G dye concentration while it rose with the boost in adsorbent dose. At pH 2.0, the highest HE4G dye deletion by adsorbent was observed. To fit the experimental equilibrium data, different isotherm models were employed. Several isotherm models, such as Langmuir, Frendlich, and Dubinin–Radushkevich models were used to determine the adsorption experimental results, but the Dubinin–Radushkevich model represented better the results than others. The highest removal percentages of HE4G dye was obtained at pH = 2.0 which was 78.3 for pure PbS, 80.9 for PbS/Mn-5%, 84.2 for PbS/Mn-10%, and 87.4% for PbS/Mn-15%. Also the highest adsorption capacities (q_{max}) were found to be about 78.74 mg/g for pure PbS, 103.9 mg/g for PbS/Mn-5%, 133.33 mg/g for PbS/Mn-10%, and 144.49 mg/g for PbS/Mn-15%. Adsorption mechanism for these adsorbents was considered to be physical which was confirmed by the E (kJ/mol) obtained from Dubinin–Radushkevich isotherm for pure PbS, PbS/Mn-5%, PbS/Mn-10%, and PbS/Mn-15% were roughly –700.0, –770.1, –817.12, and –903.0 (kJ/mol), respectively. The kinetics scrutiny decided that HE4G dye deletion followed pseudo-second-order rate equation. Thermodynamic parameters of free energy ($\Delta G°$), enthalpy ($\Delta H°$), and entropy ($\Delta S°$) of adsorption were determined using isotherms. $\Delta H°$ = –23.9 kJ/mol, $\Delta G°$ = –5.337 kJ/mol, and $\Delta S°$ = –63.3 J/mol K and $\Delta H°$ = –14.5 kJ/mol, $\Delta G°$ = –2.858 kJ/mol for PbS, and $\Delta S°$ = –38.9 J/mol K for PbS/Mn-15%. The fact that the sorption process was exothermic was well reflected by the negative value of ($\Delta G°$, $\Delta H°$, and $\Delta S°$) which on its own expressed the affinity of Mn-doped PbS (PbS:Mn) nanoparticles synthesis for deleting HE4G dye. In addition, the possibility of recycling the adsorbent was well proved by desorption studies. Based on the results from the linear regression-based analysis, it was revealed that the derived empirical models represented a passable prediction of performance for pure PbS, PbS/Mn-5%, PbS/Mn-10%, and PbS/Mn-15% nanoparticles with significant determination coefficients (R^2 = 0.994–0.984). Additionally, the statistical outcomes guaranteed that the recommended equations could favorably be employed for the adsorption of HE4G dye from aqueous solutions. As a final result, we should claim that the synthesized Mn-doped PbS (PbS:Mn) nanoparticles have a good capacity for removing HE4G dye and the other dyes from aqueous media at a low cost, available and efficient adsorbent.

Acknowledgments

The authors gratefully acknowledge partial support of this work by the Islamic Azad University, Branch of Omidiyeh Iran.

References

[1] S. Soni, P.K. Bajpai, J. Mittal, Utilisation of cobalt doped iron based MOF for enhanced removal and recovery of methylene blue dye from waste water, J. Mol. Liq., (2018), 314 (2020) 113642–113654.

[2] Aruna, N. Bagotia, A.K. Sharma, S. Kumar, A review on modified sugarcane bagasse biosorbent for removal of dyes, Chemosphere, 268 (2021) 129309–129319.

[3] C. Arora, S. Soni, S. Sahu, J. Mittal, P. Kumar, P.K. Bajpai, Iron based metal organic framework for efficient removal of methylene blue dye from industrial waste, J. Mol. Liq., 284 (2019) 373–352.

[4] I. Anastopoulos, I. Pashalidis, A.G. Orfanos, I.D. Manariotis, T. Tatarchuk, L. Sellaoui, A. Bonilla-Petriciolet, A. Mittal, A. Nunez-Delgado, Removal of caffeine, nicotine and amoxicillin from (waste) waters by various adsorbents. A review, J. Environ. Manage., 261 (2020) 110236–110244.]

[5] V. Kumar, P. Saharan, A.K. Sharma, A. Umar, I. Kaushal, Y. Al-Hadeethi, B. Rashad, A. Mittal, Silver doped manganese oxide-carbon nanotube nanocomposite for enhanced dye-sequestration: isotherm studies and RSM modelling approach, J. Ceram. Int., 46 (2020) 10309–10319.

[6] M. Alizadeh, H. Nadi, M. Ahmadabadi, A.R. Yari, S. Hashemi, Removal of reactive dyes (green, orange, and yellow) from aqueous solutions by peanut shell powder as a natural adsorbent, J. Arch. Hyg. Sci., 1 (2012) 41–47.

[7] M. Ghaedi, B. Sadeghian, A.A. Pebdani, R. Sahraei, A. Daneshfar, C. Duran, Kinetics, thermodynamics and equilibrium evaluation of direct yellow 12 removal by adsorption onto silver nanoparticles loaded activated carbon, Chem. Eng. J., 187 (2012) 133–141.

[8] A. Mittal, V. Thakur, V. Gajbe, Evaluation of adsorption characteristics of an anionic azo dye Brilliant Yellow onto hen feathers in aqueous solutions, J. Environ. Sci. Pollut. Res., 19 (2012) 2438–2447.

[9] M. Turabik, Adsorption of basic dyes from single and binary component systems onto bentonite: simultaneous analysis of Basic Red 46 and Basic Yellow 28 by first order derivative spectrophotometric analysis method, J. Hazard. Mater., 158 (2008) 52–64.

[10] I. Anastopoulos, A. Mittal, M. Usman, J. Mittal, G. Yu, A. Nunez-Delgado, M. Kornaros, A review on halloysite-based adsorbents to remove pollutants in water and wastewater, J. Mol. Liq., 269 (2018) 855–868.

[11] J. Mittal, V. Thakur, A. Mittal, Batch removal of hazardous azo dye using waste material hen feather, Ecol. Eng., 60 (2013) 249–253.

[12] A. Asfaram, M. Ghaedi, A. Goudarzi, M. Rajabi, Response surface methodology approach for optimization of simultaneous dye and metal ion ultrasound-assisted adsorption onto Mn doped Fe_3O_4-NPs loaded on AC: kinetic and isothermal studies, Dalton Trans., 44 (2015) 14707–14723.

[13] H. Daraei, A. Mittal, Investigation of adsorption performance of activated carbon prepared from waste tire for the removal of methylene blue dye from wastewater, Desal. Water Treat., 90 (2017) 294–298.

[14] A. Mittal, R. Ahmad, I. Hasan, Poly(methyl methacrylate)-grafted alginate/Fe_3O_4 nanocomposite: synthesis and its application for the removal of heavy metal ions, Desal. Water Treat., 57 (2016) 19820–19833.

[15] A. Mittal, R. Ahmad, I. Hasan, Iron oxide-impregnated dextrin nanocomposite: synthesis and its application for the biosorption of Cr(VI) ions from aqueous solution, Desal. Water Treat., 57 (2016) 15133–15145.

[16] Y. Kuang, X. Zhang, S. Zhou, Adsorption of methylene blue in water onto activated carbon by surfactant modification, Water Res., 12 (2020) 587–598.

[17] R. Gaur, P. Jeevanandam, PbS micro-nanostructures with controlled morphologies by a novel thermal decomposition approach, Nanopart. Res., 18 (2016) 80–100.

[18] K. Suresh Babu, C. Vijayan, R. Devanathan, Strong quantum confinement effects in polymer-based PbS nanostructures prepared by ion-exchange method, Mater. Lett., 58 (2004) 1223–1226.

[19] J. Liu, H. Yu, Z. Wu, W. Wang, J. Peng, Y. Cao, Size-tunable near-infrared PbS nanoparticles synthesized from lead carboxylate and sulfur with oleylamine as stabilizer, Nanotechnology, 19 (2008) 19 (2008) 345602–345614.

[20] E. Yücel, Y. Yücel, Fabrication and characterization of Sr-doped PbS thinfilms grown by CBD, Ceram. Int. J., 43 (2017) 407–413.

[21] G. Long, B. Barman, S. Delikanli, Y. Tsung Tsai, P. Zhang, A. Petrou, H. Zeng, Carrier-dopant exchange interactions in Mn-doped PbS colloidal quantum dots, Appl. Phys. Lett., 101 (2012) 62410–62422.

[22] J.B. Pendry, A.J. Holden, D.J. Robbins, W.J. Stewart, Magnetism from conductors and enhanced non-linear phenomena, IEEE Trans. Microwave Theory Tech., 47 (1999) 2075–2084.

[23] D.R. Smith, W.J. Padilla, D.C. Vier, S.C. Nemat-Nasser, S. Schultz, Composite medium with simultaneously negative permeability and permittivity, Phys. Rev. Lett., 84 (2000) 4184–4187.

[24] J.B. Pendry, Negative refraction makes a perfect lens, Phys. Rev. Lett., 85 (2000) 3966–3969.

[25] W.P. Utomo, E. Santoso, G. Yuhaneka, A.I. Triantini, M.R. Fatqi, M.F. Hudadan, N. Nurfitria, Studi adsorpsi zat warna naphthol yellow s pada limbah cair menggunakan karbon aktif dari ampas tebu, J. Chem., 13 (2019) 104–116.

[26] A.N. Chattarki, S.S. Kamble, L.P. Deshmukh, Role of pH in aqueous alkaline chemical bath deposition of lead sulfide thin films, Mater. Lett., 67 (2012) 39–41.

[27] H. Mahmoudi Chenari, B. Ramezanpour, H. Kangarlou, Metamaterial Mn-doped PbS nanoparticles: synthesis, size-strain linebroadening analysis and Kramers–Kronig study, Ceram. Int., 6 (2017) 109–122.

[28] H.S. Ghazi Mokri, N. Modirshahla, M.A. Behnajady, B. Vahid, Adsorption of C.I. Acid Red 97 dye from aqueous solution onto walnut shell: kinetics, thermodynamics parameters, isotherms, Int. J. Environ. Sci. Technol., 12 (2015) 1401–1408.

[29] Y. Zhao, J. Zou, W. Shi, *In situ* synthesis and characterization of PbS nano crystallites in the modified hyperbranched polyester by gamma-ray irradiation, J. Mater. Sci. Eng., 121 (2005) 20–24.

[30] T.S. Shyju, S. Anandhi, R. Sivakumar, R. Gopalakrishnan, Studies on lead sulfide (PbS) semiconducting thin films deposited from nanoparticles and its NLO application, Int. J. Nanosci., 13 (2014) 1450001–1450012.

[31] F. Gode, O. Baglayan, E. Guneri, P-Type nano structure PbS thin films prepared by the silar method, Chalcogenide. Lett., 12 (2015) 519–528.

[32] W. Wei, L. Yang, W.H. Zhong, S.Y. Li, J. Cui, Z.G. Wei, Fast removal of methylene blue from aqueous solution by adsorption onto poorly crystalline hydroxyapatite nanoparticles, Nanomater. Biostruct., 10 (2015) 1343–1363.

[33] B. da Silva, A. Zanutto, Biosorption of reactive yellow dye by malt bagasse, Adsorpt. Sci. Technol., 37 (2019) 236–259.

[34] M. Kiani, S. Bagheri, N. Karachi, E. Alipanahpour Dil, Adsorption of purpurin dye from industrial wastewater using Mn-doped Fe_2O_4 nanoparticles loaded on activated carbon, Desal. Water Treat., 60 (2019) 1–8.

[35] A. Naghizadeh, M. Kamranifar, Montmorillonite nanoparticles in removal of textile dyes from aqueous solutions: study of kinetics and thermodynamics, Iran. J. Chem. Eng., 36 (2017) 127–137.

[36] S. Hajati, M. Ghaedi, H. Mazaheri, Removal of methylene blue from aqueous solution by walnut carbon: optimization using response surface methodology, Desal. Water Treat., 57 (2016) 3179–3193.

[37] R. Mahini, H. Esmaeili, R. Foroutan, Adsorption of methyl violet from aqueous solution using brown algae Padina sanctae-crucis, Turk. J. Biochem., 24 (2018) 1–9.

[38] I. Langmuir, The adsorption of gases on plane surfaces of glass, mica and platinum, J. Am. Chem. Soc., 40 (1918) 1361–1403.

[39] H.M.F. Freundlich, Over the adsorption in solution, J. Phys. Chem., 57 (1906) 385–470.

[40] N.D. Hutson, R.T. Yang, Theoretical basis for the Dubinin–Radushkevitch (D–R) adsorption isotherm equation, Adsorption, 3 (1997) 189–195.
[41] M.M. Dubinin, Modern state of the theory of volume filling of micropore adsorbents during adsorption of gases and steams on carbon adsorbent, Z. Fiz. Khim., 39 (1965) 1305–1317.
[42] M. Toor, B. Jin, Adsorption characteristics, isotherm, kinetics, and diffusion of modified natural bentonite for removing diazo dye, Chem. Eng. J., 187 (2012) 79–88.
[43] Y.S. Ho, Review of second-order models for adsorption systems, J. Hazard. Mater., 136 (2006) 681–689.
[44] F. Bouaziz, M. Koubaa, F. Kallel, R.E. Ghorbel, S.E. Chaabouni, Adsorptive removal of malachite green from aqueous solutions by almond gum: kinetic study and equilibrium isotherms, Int. J. Biol. Macromol., 105 (2017) 56–65.
[45] S. Banerjee, G.C. Sharma, R.K. Gautam, M.C. Chatto Padhyaya, S.N. Upadhyay, Y.C. Sharma, Removal of malachite green, a hazardous dye from aqueous solutions using *Avena sativa* (oat) hull as a potential adsorbent, J. Mol. Liq., 213 (2016) 162–172.
[46] S. Hajati, M. Ghaedi, B. Barazesh, F. Karimi, R. Sahraei, A. Daneshfar, A. Asghari, Application of high order derivative spectrophotometry to resolve the spectra overlap between BG and MB for the simultaneous determination of them: ruthenium nanoparticle loaded activated carbon as adsorbent, Ind. Eng. Chem., 20 (2014) 2421–2427.
[47] A. Achmad, J. Kassim, T. Kim Suan, Equilibrium, kinetic and thermodynamic studies on the adsorption of direct dye onto a novel green adsorbent developed from Uncaria gambir extract, Phys. Sci., 23 (2012) 1–13.
[48] R. Manohar, V.S. Shrivastava, Adsorption removal of carcinogenic acid violet19 dye from aqueous solution by polyaniline-Fe_2O_3 magnetic nano-composite, Mater. Environ. Sci., 6 (2015) 11–21.